Journal of Computational Physics **172,** 309–325 (2001)
doi:10.1006/jcph.2001.6825, available online at http://www.idealibrary.com on IDEAL®

On Spurious Vortical Structures

Dimitris Drikakis* and Piotr K. Smolarkiewicz†

**Queen Mary, University of London, Engineering Department, London E1 4NS, United Kingdom; and*
†European Centre for Medium-Range Weather Forecasts, Reading, United Kingdom,
and National Center for Atmospheric Research Boulder, Colorado 80307
E-mail: d.drikakis@qmw.ac.uk; smolar@ncar.ucar.edu

The paper investigates the formation of spurious vortical structures in incompressible flow simulations employing Godunov-type methods. The present work is motivated by the earlier studies of Brown and Minion (1995, *J. Comput. Phys.* **122**, 165 and 1997, *J. Comput. Phys.* **138**, 734) who demonstrated for a variety of numerical schemes (and for the upwind-biased methods in particular) that spurious vortices can occur in underresolved flow simulations. The aim of our work is threefold: (i) to identify deficiencies in various Godunov-type methods leading to spurious flow structures, (ii) to examine the numerical mechanisms responsible for these artifacts, and (iii) to propose modifications of Godunov-type methods in order to recover the correct solutions even under insufficient grid resolution. Our results reveal that the occurrence of spurious solutions depends strongly on the Godunov-type method employed. We show that in addition to the dissipation properties of a scheme—emphasized by Brown and Minion—there are other factors that can also contribute to numerical artifacts. These include a vortical instability arising from the numerical discretization of the advective terms in the primitive variable formulation of the Navier–Stokes equations, the balance of dissipation among the different discretized terms in a Godunov-type method, as well as order of accuracy of the interpolation used to discretize the wave-speed dependent term of the Godunov flux.

Key Words: finite volume; Godunov-type methods; unsteady incompressible flows.

1. INTRODUCTION

Brown and Minon [1, 2] have documented, for various numerical methods, a class of numerical artifacts ("spurious eddies") that occur in underresolved simulations of two-dimensional (2D) incompressible vortex-street flows. In [1], they showed that the second-order Godunov-projection method of Bell *et al.* [3] leads to spurious eddies for simulations performed on relatively coarse grids. In [2], they explored several numerical methods including the Godunov-projection, a primitive variable ENO, a pseudo-spectral, as well as upwind

0021-9991/01 $35.00

and centered vorticity/stream-function methods. There, they showed that the formation of spurious vortices can occur with all methods[1] if the grid resolution is insufficient; however, upwind-biased schemes, such as the second-order Godunov-projection method, require higher resolution to avoid spurious eddies. Furthermore, they suggested that the addition of artificial viscosity can prevent these vortices even on coarse grids, but at the expense of more diffusive solutions. They argued that these artifacts are not a high wavenumber effect, but rather represent the growth of unstable low wavenumber perturbations introduced by the truncation error of the methods.

Our work is motivated by Brown and Minion's [1, 2] studies. In general, we seek an understanding of the numerical mechanisms underlying the formation of spurious vortical structures in underresolved flows. Using heuristic vorticity arguments, we identify specific terms of the truncation error responsible for the spurious solutions. This guides us toward modifications of the Godunov-type methods that attain correct physical solutions even when coarse grids are employed.

The assumed physical/mathematical scenario is quite elementary: the evolution of a 2D vortex street in a homogeneous incompressible fluid on a doubly periodic unit-square domain, described by the standard incompressible Navier–Stokes equations,

$$\begin{aligned} \frac{\partial u_i}{\partial x_i} &= 0 \\ \frac{\partial u_i}{\partial t} + \frac{\partial u_i u_j}{\partial x_j} &= -\frac{\partial p}{\partial x_i} + \frac{1}{Re}\Delta u_i . \end{aligned} \tag{1}$$

Here, $u_i (i = 1, 2$ refers to the space coordinates $x, y)$ are the velocity components, p is the pressure, Re is the Reynolds number, and t is the time; all variables are properly normalized. The particular flow simulated is that proposed in [3] and studied extensively in [1, 2]. The initial condition consists of a double shear layer

$$u = \begin{cases} \tanh((y - 0.25)\delta) & \text{if} \quad y \le 0.5 \\ \tanh((0.75 - y)\delta) & \text{if} \quad y > 0.5, \end{cases} \tag{2}$$

where δ determines the shear layer thickness that is weakly perturbed in the spanwise direction. Such a flow is hydrodynamically unstable (see e.g., [5], Chapter 7.1) and, therefore, one may expect different flow realizations depending on the initial perturbation. Subsequently, this can affect the response of numerical schemes employed—especially the response of the nonlinear schemes such as Godunov-type methods—and any spurious solutions associated with it. In order to reduce the investigated area of the solution space to a necessary minimum, here (as in [1, 2, 3]) we will consider only a sinusoidal perturbation of the spanwise velocity

$$v = v' \sin(2\pi x), \tag{3}$$

where v' is the perturbation amplitude. As defined, the problem has the converged solution that takes the familiar form of a regular vortex street (Fig. 1a)—an apparent manifestation of the unstable wave-number-one mode. The spurious solutions evince a secondary eddy

[1] Recently, Tolstykh and Chigirev [4] showed that compact schemes implemented in the framework of the vorticity/stream-function formulation also result in spurious eddies.

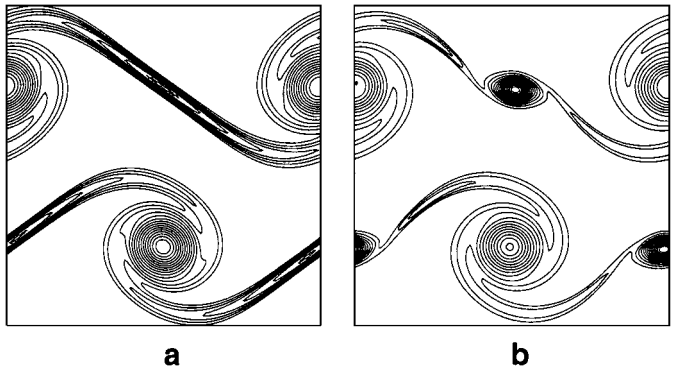

FIG. 1. (a) Correct and (b) spurious solutions for the problem of the double shear-layer; The results correspond to $Re = 10000$, $\delta = 100$, $v' = 0.05$ at dimensionless time $t = 1$.

embedded between the two primary vortices (Fig. 1b), thus manifesting a slower growth of the nonlinearly generated wave-number-two mode. Qualitatively, the relative growth rate of the two modes is consistent with the development of shear-gravitational instabilities [6], where the longer wavelengths amplify faster in the nonlinear regime of the flow. The spurious numerical solution is physically realizable, and perhaps even preferred in a laboratory scenario, as for a solenoidal white-noise initial perturbation, our experiments showed that all solutions evince the secondary eddy. However, for a fixed Reynolds number and the sole excitation of the primary mode, the spurious vortices do disappear when the grid is sufficiently refined, for all methods considered in this paper. The details of this convergence depend both on the Reynolds number and the advective scheme employed. Thus, although the problem may be somewhat academic from the physical viewpoint—as bifurcated solution are admissible (cf. [7, 8], for a discussion)—it forms an interesting testbed for numerical methods in CFD, especially since it seems to elude clear understanding.[2]

A series of numerical experiments performed in this study using various Godunov-type methods showed that the generation of spurious eddies depends strongly on how the numerical dissipation is partitioned between different terms of the advective scheme. As in [2], we have found that both centered and upwind methods can lead to spurious solutions. Furthermore, our numerical experiments revealed that in the case of centered-differencing-based Godunov methods, spurious vortices may or may not appear depending on the detailed form of the Godunov flux. The latter shows that not all Godunov-type methods result in spurious vortices.

We have augmented our experiments focused on Godunov-type methods with an auxiliary study (to be reported elswhere) using the nonoscillatory-forward-in-time (NFT) approach of Smolarkiewicz and Margolin [9]. The NFT approach is based on upwind-biased methods, but can employ optionally either Eulerian (viz., flux-form) [11] or semi-Lagrangian (viz. advective) form [12] finite-difference approximations for the governing equations of motion. These experiments reveal that semi-Lagrangian (i.e., trajectory wise) integrals tend to produce correct solutions as in Fig. (1a), whereas Eulerian (i.e., control-volume wise) integrals tend to evince the secondary eddy (cf. Fig. 1b). Our experience with the NFT methods is that the Eulerian option is more accurate/effective in applications in which the physics of

[2] To our knowledge there has been no investigation of spurious eddies in 3D flows—likely because of the prohibitive computational expense of the 3D convergence studies for a range of methods.

the problem depends on a detailed balance of the momentum fluxes. This contrasts with the semi-Lagrangian option, which appears more accurate/effective for problems governed by vorticity dynamics; cf. [13]. The latter observation, coupled with the results from the NFT simulations, have suggested a vorticity analysis of the discretized momentum equations in the context of Godunov-type methods.

A rigorous vorticity analysis of nonlinear approximations, such as of the high-order Godunov-type (or NFT) schemes, appears hopeless. To illuminate the issue, we offer instead heuristic vorticity arguments with the essentials of the Godunov-type methods in mind. These arguments suggest that reducing the order of accuracy in the discretization of the wave-speed dependent term of the Godunov flux (henceforth labeled WST; see also Sec. 2.1) should counteract the formation of spurious eddies. Numerical experiments corroborate this deduction. Discretizing WST using first-order-accurate interpolation corrects the numerical solution of all those Godunov-type methods that previously led to spurious vortical structures. Although the exact numerical mechanism responsible for the generation and disappearance of the spurious eddy is not fully understood, we appreciate that reducing the order of accuracy of the discretized WST term modifies the nonlinear dissipation of the Godunov-type methods. To assess the effects of the modified WST on the accuracy of the methods, we present error estimation for the original and modified schemes in different flow problems including the one in question.

The paper is organized as follows. In Section 2, we outline the computational framework and summarize briefly the Godunov-type methods employed. In Section 3, we discuss solutions obtained by different Godunov-type methods. In Section 4, we present a vorticity analysis that aims at explaining the formation of spurious solutions, and propose a remedy for suppressing the spurious eddies in Godunov-type methods. We conclude our study in Section 5.

2. NUMERICAL FRAMEWORK AND GODUNOV-TYPE METHODS

The numerical framework exploited in this study is the incompressible Navier–Stokes solver described in [14, 15]. Below we comment briefly on the essential aspects of the design of the solver while referring the reader to the earlier work for further details.

To take full advantage of the Godunov methods designed for hyperbolic conservation laws, the incompressible equations (1) are cast in a compressible format by means of the artificial-compressibility approach. The classical formulation of Chorin [16], suitable for steady-state problems, is extended to transient flows [17–20] via an approach referred sometimes to as dual-time stepping. The overall idea of the dual-time stepping can be summarized as follows:[3] At each instant t, the augmented pseudo-compressible system,

$$\begin{aligned} \frac{1}{\beta}\frac{\partial p}{\partial \tau} + \frac{\partial u_i}{\partial x_i} &= 0 \\ \frac{\partial u_i}{\partial \tau} + \frac{\partial}{\partial x_j}(u_i u_j + p\delta_{ij}) &= -\alpha(u_i - \tilde{u}_i) + \frac{1}{Re}\Delta u_i, \end{aligned} \tag{4}$$

[3] An alternate summary could be given in terms of the implicit discretization of the system (1) with the Euler-backward scheme, forming the system of nonlinear Helmholtz equations, and solving it iteratively by augmenting the elliptic problem with a pseudo-time integration (cf. [10]).

is integrated in a pseudo-time τ to a steady state, assuming an artificial speed of sound $\sqrt{\beta}$.[4] Here, $\tilde{u}_i$ denotes the solution at the instant t, whereas all tilde-free variables are allowed (in principle) to vary in the pseudo-time $\tau \in [t,\ t + \Delta t]$. The attenuation forcing on the right-hand side (rhs) of the momentum equation damps the flow divergence to zero (given $\partial \tilde{u}_i / \partial x_i = 0$) at the rate $\alpha \equiv (\Delta t)^{-1}$. In the steady state at $\tau = t + \Delta t$, all $\partial / \partial \tau$ terms vanish and the damping term on the rhs becomes the $\partial u_i / \partial t$ derivative of the Godunov scheme at hand, i.e., the u_i solution becomes the $\tilde{u}_i$ solution at $t + \Delta t$. In our model the default time integration with respect to τ employs a fourth-order Runge–Kutta scheme [21] (selected, primarily, for the optimum performance on nonuniform grids) while a nonlinear multigrid method [14] is used to accelerate the convergence toward the steady state. The viscous terms are discretized by standard central differences. The reader interested in further analysis of the artificial-compressibility approach is referred to [24].

In order to establish whether any other part of the algorithm, apart from the discretization of the advective terms, contributes to spurious solutions, we performed calculations using the first-order Euler-forward as well as second- and third-order Runge–Kutta [21] time-stepping schemes both with and without the multigrid accelerator. The results revealed that neither the multigrid algorithm nor the order of the time-stepping (Euler or Runge–Kutta) scheme alter the numerical solution, thereby supporting the conclusion that from the algorithmic point of view, the formation of spurious vortices depends solely on the advective scheme employed. This is corroborated by the results of the auxiliary experiments with semi-Langrangian and Eulerian NFT schemes (see Introduction) which indicate that the issue is unrelated to a truncation-error violation of vector differentiation identities ($\nabla \times \nabla p = 0$, in particular; cf. [22, 23]) as both variants of the NFT algorithms differ only, but essentially, in representing advective transport on the grid.

For further reference, let us focus attention on the x-direction advective flux in all three equations of the system (4):

$$E \equiv \begin{pmatrix} u \\ u^2 + p \\ uv \end{pmatrix}. \tag{5}$$

In all Godunov methods considered in this study, the advective flux derivative $\partial E / \partial x$ is discretized at the center of the control volume (i, j) using the values of the intercell fluxes, i.e., $\partial E / \partial x = (E_{i+1/2,\,j} - E_{i-1/2,\,j})/\Delta x$. To simplify the notation, the subscript j will be omitted throughout the rest of paper. The definition of the intercell flux function distinguishes among the different Godunov-type methods implemented in this study within the artificial-compressibility framework (4).

2.1. *Rusanov Scheme [25]*

The Rusanov flux (henceforth labeled RU) at a cell face $(i + 1/2)$ is given by

$$E_{i+1/2} = \frac{1}{2}(E_L + E_R) - \frac{1}{2} S^+ (U_R - U_L), \tag{6}$$

where $E_L = E_L(U_L)$ and $E_R = E_R(U_R)$ denote the left and right states of the flux, respectively, at the cell face of the computational volume; cf. [25, 26]. Similarly, U_L and

[4] The artificial compressibility parameter is $\beta \equiv 1$ throughout this study.

U_R are the left and right states, respectively, of the vector of the primitive variables U = $U = (p, u, v)^T$ at the cell face of the computational volume. The second term in the rhs of (6) is the wave-speed dependent term (WST). Following Davis [27], the speed S^+ is defined as the maximum wave speed, i.e.,

$$S^+ = max(|u_L - s_L|, |u_R - s_R|, |u_L + s_L|, |u_R + s_R|), \tag{7}$$

where, in the context of the artificial-compressibility approach, $s = \sqrt{u^2 + \beta}$. For the calculation of the left and right states we employ nonoscillatory interpolation for the primitive variables (see Section 2.6).

2.2. *Lax–Friedrichs Scheme [28]*

If in the Rusanov flux one defines S^+ as the maximum wave speed found by imposing the Courant–Friedrichs–Lewy (CFL) stability condition—i.e., $S^+ = S_{max} = C\Delta x/\Delta t$, where C is the CFL number—then, for $C = 1$, one obtains the Lax–Friedrichs flux (henceforth labeled LF):

$$E_{i+1/2} = \frac{1}{2}(E_L + E_R) - \frac{1}{2}\frac{\Delta x}{\Delta t}(U_R - U_L). \tag{8}$$

2.3. *Einfeldt's Scheme [29]*

Einfeldt's HLLE scheme [29] is an extension of the Harten–Lax–van Leer (HLL) scheme [30]. The central idea of the HLL scheme is to assume a particular wave configuration for the solution, consisting of two waves separating three constant states. Assuming that the wave speeds are defined through a given algorithm, one can apply the integral form of the conservation laws and obtain an approximate expression for the flux. The difference between the original HLL scheme [30] and its HLLE version lies in the way the wave speeds are calculated. According to the HLLE scheme, the flux E is defined by

$$E_{i+1/2} = \frac{b^+_{i+1/2}E_L - b^-_{i+1/2}E_R}{b^+_{i+1/2} - b^-_{i+1/2}} + \frac{b^+_{i+1/2}b^-_{i+1/2}}{b^+_{i+1/2} - b^-_{i+1/2}}(U_R - U_L), \tag{9}$$

where $b^+_{i+1/2} = max((\lambda_1)_i, (\lambda_1)_{i+1})$ and $b^-_{i+1/2} = min((\lambda_2)_i, (\lambda_2)_{i+1})$. In the context of the artificial-compressibility approach, the eigenvalues λ_1 and λ_2 are given by

$$\lambda_1 = u + \sqrt{u^2 + \beta}, \qquad \lambda_2 = u - \sqrt{u^2 + \beta}. \tag{10}$$

The Rusanov flux can also be obtained from (9) if $b^-_{i+1/2} = -b^+_{i+1/2}$ and $b^+_{i+1/2}$ is defined by (7) [27].

2.4. *First-Order Centered Scheme [31]*

The first-order centered scheme (FORCE) proposed by Toro [26, 31] is written as the arithmetic average of the Richtmyer and Lax–Friedrichs schemes. The cell-face flux is given by

$$E_{i+1/2} = \frac{1}{2}\left(E^{RI}_{i+1/2} + E^{LF}_{i+1/2}\right), \tag{11}$$

where E^{RI} and E^{LF} denote the Richtmyer and Lax–Friedrichs fluxes, respectively. The Richtmyer flux is given by

$$E_{i+1/2} = E\left(U_{i+1/2}^{m+1/2}\right), \tag{12}$$

where

$$U_{i+1/2}^{m+1/2} = \frac{1}{2}\left(U_R^m + U_L^m\right) - \frac{1}{2}\frac{\Delta t}{\Delta x}\left(E_R^m - E_L^m\right). \tag{13}$$

In the original FORCE [26, 31], R and L appearing on the rhs of (13) and (8) refer to $i+1$ and i, respectively. The original scheme was developed for compressible flows, where $m+1/2$ in (12) and (13) denotes a half-time level between two consecutive physical time instants. In the context of the pseudo-compressible system (4), $m+1/2$ denotes an intermediate pseudo-time level between τ and $\tau + \Delta\tau$.

2.5. *Uniformly High-order (UHO) Scheme [15]*

The uniformly high-order (UHO) scheme for incompressible flows [15], draws from the ideas underlying the essentially nonoscillatory (ENO) approach [32, 33]. It aims at increasing the accuracy of the intercell fluxes via a high-order interpolation (flux reconstruction) procedure, that can be briefly summarized as follows.

A characteristic-based scheme [7, 34, 35] is initially used to provide a first approximation for the advective flux E_i at the cell centers i. Then, the cell-centered approximated fluxes are interpolated to provide high-order accurate left (E_L) and right (E_R) intercell fluxes. For example, the E_R flux is defined as

$$(E_R)_{i+1/2} = \sum_{k=-r+3-n}^{r-2} \alpha_k^r E_{i+k}, \tag{14}$$

where: r denotes the order of accuracy of the resulting scheme, with $n = 0\ \forall\, r > 3$ and $n = 1$ if $r = 3$; and the coefficients α_k^r are *constant* weights defined by an analytic procedure that minimizes the numerical dissipation and dispersion [15]. In the present study, we have employed the third-order version of the scheme for which the values of the coefficients are: $\alpha_0 = 5/6$, $\alpha_1 = -1/6$, and $\alpha_{-1} = 1/3$. This high-order interpolation can be retained throughout the computations only in the case of periodic boundaries (present problem); in the vicinity of solid boundaries the second-order-accurate scheme would be used.

Finally, the left and right intercell fluxes are combined using the Lax–Friedrichs scheme (8) to calculate the new intercell flux $E_{i+1/2}$, which is subsequently used in the discretization of the advective flux derivative.

2.6. *Cell-face Evaluation of U_L and U_R*

All listed Godunov-type methods require calculations of left and right states of the primitive variables, U_L and U_R, at the cell faces. In this paper, two interpolation schemes have

been employed: (a) the "third-order" Lagrangian interpolator[5]

$$U_L = \frac{1}{6}(5U_i - U_{i-1} + 2U_{i+1}), \qquad U_R = \frac{1}{6}(5U_{i+1} - U_{i+2} + 2U_i), \tag{15}$$

and (b) the MUSCL scheme [37]. MUSCL defines the left and right states as

$$U_L = U_i + \frac{g_i}{4}[(1 - kg_i)\nabla + (1 + kg_i)\Delta]U_i \tag{16}$$

$$U_R = U_{i+1} - \frac{g_{i+1}}{4}[(1 + kg_{i+1})\nabla + (1 - kg_{i+1})\nabla]U_{i+1}. \tag{17}$$

Parameter k controls different MUSCL realizations: fully upwind for $k = -1$, third-order for $k = 1/3$,[6] and centered for $k = 1$; g_i is the van Albada limiter [38]

$$g_i = \frac{2\nabla U_i \Delta_i U_i}{(\nabla U_i)^2 + (\Delta U_i)^2 + \epsilon}. \tag{18}$$

In (16)–(18), $\nabla U_i = U_i - U_{i-1}$, $\Delta U_i = U_{i+1} - U_i$, and ϵ is a small positive constant preventing division by zero.

3. SPURIOUS SOLUTIONS

Here, we substantiate our earlier assertion (see Introduction) that the occurrence of the spurious eddies in the vortex-street simulations (Fig. 1) depends strongly on the advective scheme employed. We have used the Godunov-type methods listed in the preceding section in conjunction with either the Lagrangian interpolation (15) or different variants of the MUSCL scheme. All simulations were performed on both the "coarse" (128×128) and the "fine" (256×256) grid. In order to confirm the convergence of the fine-grid solutions, selected simulations have been repeated on the 512×512 grid.[7] Together this has led to a large series of numerical experiments gathering a systematic evidence on the response of various schemes. All experiments assumed a Reynolds number $Re = 10000$ in (1), the thickness of the shear layer $\delta = 100$ in (2), and the amplitude of the initial spanwise perturbation $v' = 0.05$ in (3). Depending on the Reynolds number and the thickness of the shear layer,[8] the number of vortices can be increased or reduced [1–3]. The larger the δ, the more likely is the occurrence of the spurious solutions. Here, we consider a relatively thin layer to emphasize the development of the spurious eddies—in [1, 2], $\delta = 80$ and $\delta = 100$ were employed.

The results of 48 numerical experiments regarding the occurrence of the spurious eddy are summarized in Table I. Representative results of both correct and spurious solutions on the coarse grid are also shown in Fig. 2. In the table, the variants of the MUSCL scheme are labeled as *MUFU* (corresponding to $k = -1$), *MU3* (corresponding to $k = 1/3$), and *MUC* (corresponding to $k = 1$). Simulations using the Lagrangian interpolator (15) are labeled

[5] Note that the interpolation in (15) is not third-order accurate per se, but it ensures third-order accuracy of the WST term $(U_R - U_L)$, [36].

[6] For $k = 1/3$, the scheme is strictly third order only for one-dimensional problems.

[7] The reader interested in the morphology of highly resolved solutions and its implications for the mechanics of the spurious eddies is referred to [39].

[8] Note that larger δ leads to a thinner shear layer.

TABLE I

Response of Various Godunov-Type Schemes with Respect to the Occurrence of Spurious Vortical Structures, for the Double Shear Layer Problem ($Re = 10000$, $\delta = 100$, $v' = 0.05$)

Scheme	128×128	256×256
RU-L3	Correct	Correct
RU-MUFU	Correct	Correct
RU-MU3	Correct	Correct
RU-MUC	Correct	Correct
UHO-L3	Spurious	Correct
UHO-MUFU	Spurious	Correct
UHO-MU3	Spurious	Correct
UHO-MUC	Spurious	Correct
LF-L3	Correct	Correct
LF-MUFU	Correct	Correct
LF-MU3	Correct	Correct
LF-MUC	Correct	Correct
FORCE-L3	Spurious	Correct
FORCE-MUFU	Spurious	Correct
FORCE-MU3	Spurious	Correct
FORCE-MUC	Spurious	Correct
FORCE-L3^2	Correct	Correct
FORCE-MUFU^2	Correct	Correct
FORCE-MU3^2	Correct	Correct
FORCE-MUF^2	Correct	Correct
HLLE-L3	Correct	Correct
HLLE-MU3	Correct	Correct
HLLE-MUC	Correct	Correct
HLLE-MUF	Correct	Correct

Note. See the text for the definition of acronyms.

with "L3." For example, RU-MUFU and RU-L3 denote the Rusanov flux in conjunction with the fully upwind MUSCL and "third-order" Lagrangian interpolation, respectively. For the FORCE scheme, in particular, different variants can be constructed if the MUSCL or L3 interpolators are implemented in both the E^{RI} and E^{LF} fluxes (see Eq. (11)), or in only one of them. Our numerical experiments revealed that the first term, on the rhs of (8), of the flux E^{LF} in (11) must be calculated by higher-order interpolation, otherwise the solutions become overly diffusive (yet spurious-eddy free). In the Table I, an exponent "2" indicates wherever higher-order interpolation is also used in the flux E^{RI} in (11); recall that the original FORCE scheme [26, 31] employed the first-order interpolation both for the E^{RI} and E^{LF} fluxes.

Table I supports interesting conclusions. We draw attention to several points of special note:

- With the selected Re, δ, and v', all analyzed schemes yield the correct solution on the fine grid.
- The spurious-eddy-wise performance of a Godunov-type method does not depend on whether the "third-order" Lagrangian or MUSCL interpolation are employed.

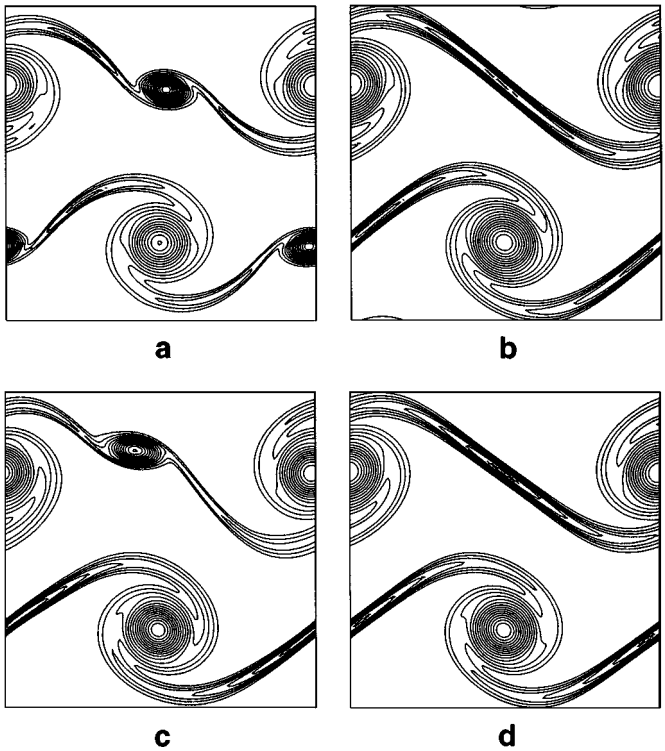

FIG. 2. Representative results from spurious and correct solutions obtained by different Godunov-type methods: (a) UHO-L3, (b) RU-L3, (c) FORCE-L3, and (d) HLLE-L3.

- The Rusanov (RU), Lax–Friedrichs (LF), and HLLE schemes do not evince spurious eddies even on the coarse grid.
- Although RU, LF, and FORCE schemes have substantial similarities—none of them requires solving the Riemann problem, and they all qualify as centered schemes—the variants FORCE-L3, FORCE-MU3, FORCE-MUFU, and FORCE-MUC exhibit different behavior. In addition to the spurious solution, they exhibit a slight asymmetry (the spurious eddy is shifted to the left). Thus, the centered schemes appear less prone, but not uniformly immune, to developing spurious vortical structures—a corroboration of the earlier results on the centered-schemes [1, 2, 40].
- Higher-order interpolation of the Godunov flux within a computational stencil has no direct impact on the occurrence of the spurious eddies. For example, the third-order version of the UHO results in spurious vortices despite the higher accuracy of interpolation.
- All FORCE schemes that use higher-order interpolation in the E^{RI} flux in (11) are less diffusive than the equivalent schemes with the first-order interpolation employed for E^{RI}, yet they evince no spurious eddies. This contrasts with the opinion (e.g., [2]) that increasing artificial viscosity remedies spurious eddies. Apparently, both increasing or decreasing artificial viscosity may prevent or excite spurious eddies.

The collected observations elude a clear explanation of the spurious solutions. In particular, the classification of Godunov-type methods as centered or upwind is insufficient to explain the tendency of a scheme toward spurious eddies; and the spurious solutions that appear in coarse-grid simulations cannot be mitigated by simply increasing the accuracy

of the advective scheme.[9] Furthermore, the auxiliary computations with the NFT methods (not shown; see Introduction) suggest that formally a less-accurate advective-form scheme can result in a correct solution while a related and more accurate flux-form algorithm may still evince spurious eddies.

At this stage, we speculate that the results depend on the nonlinear dissipation of the vorticity whose details, in turn, depend on the the momentum flux formulation. In different Godunov-type fluxes, this may or may not lead to a vortex instability. In the next section, we exploit an idealized analytic model to assess the effects of numerical discretization on the production of spurious vorticity.

4. VORTICITY ARGUMENTS AND NUMERICAL MODIFICATIONS

4.1. *Vorticity Arguments*

In order to assess the impact of discretizing the momentum equation on vorticity generation, we consider the inviscid system in (1). Using an explicit discretization in time while retaining a continuous representation in space leads to an idealized algorithm,

$$u^{n+1} = u^n - \Delta t\left(\tilde{u}\frac{\partial u}{\partial x} + \tilde{v}\frac{\partial u}{\partial y} + \frac{\partial p}{\partial x}\right) \tag{19}$$

$$v^{n+1} = v^n - \Delta t\left(\tilde{u}\frac{\partial v}{\partial x} + \tilde{v}\frac{\partial v}{\partial y} + \frac{\partial p}{\partial y}\right), \tag{20}$$

where $\tilde{u}$ and $\tilde{v}$ identify the advective (as opposed to advected) velocities. Differentiating (19) in y and (20) in x, subtracting the second equation from the first, adding and subtracting the terms $u_y\tilde{u}_x$ and $v_x\tilde{v}_y$, and using the mass continuity relation $\tilde{u}_x + \tilde{v}_y = 0$, gives the vorticity equation

$$\frac{\omega^{n+1} - \omega^n}{\Delta t} + \tilde{\mathbf{u}} \cdot \boldsymbol{\nabla}\omega = (\tilde{u}_x u_y - u_x\tilde{u}_y) + (\tilde{v}_x v_y - v_x\tilde{v}_y). \tag{21}$$

In the continuous model, $\tilde{\mathbf{u}} = \mathbf{u}$ so both terms on the rhs of (21) vanish identically, leaving the correct time-discretized vorticity equation for ideal 2D flows. In discrete models, however, $\tilde{\mathbf{u}} \neq \mathbf{u}$ in general, and the two terms on the rhs of (21) do not vanish. Typically, $\tilde{\mathbf{u}} = \mathbf{u} + \mathcal{O}(\Delta x^2)$, and the artificial vorticity source appears at the second order. This by no means implies that suppressing the source necessarily requires a fully third-order accurate discretization of the momentum equation in (1). Favorable cancellations can adequately reduce the amplitude of the source at the lower order, as illustrated by our results generated with Godunov-type methods (preceding section).

To illustrate the sensitivity of the solutions to details of the discretization, one can perform a variety of numerical experiments of greater or lesser degree of practical relevance. For instance, using a fully nonstaggered mesh, with standard centered differences for discretizing $\mathbf{u}\nabla\mathbf{u}$ terms in the nonconservative form of the momentum equation, gives a standard oscillatory algorithm rarely used in high-speed flow applications. Yet, this scheme yields zero vorticity source on the rhs of (21), and reproduces the correct solution in our simulations of the vortex street even at the coarse grid. However, just smoothing out the advective

[9] This is similar to the results obtained in [2] for calculations based on pseudo-spectral and ENO methods.

velocity with the standard 1-2-1 low-pass filter [i.e., $\phi_i^{filtered} = 0.25(\phi_{i+1} + 2\phi_i + \phi_{i-1})$] suffices to form the spurious eddy. Another standard centered scheme that uses the flux form of the momentum equation, with fluxes defined at the cell faces via arithmetic averaging, also results in the spurious eddy. Since modern flux-form schemes tend to exploit the difference between the advective and advected velocities, they are more prone to form artificial vorticity sources than the advective-form algorithms.

For simple algorithms such as standard centered differences, it is tedious but feasible to derive the complete finite-difference vorticity equation implied by the discrete momentum equation, and to expose the explicit form of the error on the rhs of (21). In the case of complicated algorithms such as Godunov-type methods, this seems a hopeless task. However, some insights can be obtained if one attempts to pursue heuristic vorticity arguments with the general form of the Godunov flux

$$E_{i+1/2} = \frac{1}{2}(E_L + E_R) - \frac{1}{2}|A|(U_R - U_L), \tag{22}$$

where A approximates $\partial E/\partial U$ (the entries of the Jacoby matrix, in general).

When considered in the context of the momentum equations, the first term on the rhs of (22) is, in essence, a nondissipative centered-in-space finite-difference approximation to the momentum flux. In the implied vorticity equation, this term will tend to generate spurious sources as those observed in the experiments with elementary centered flux-form schemes. The second, WST, term on the rhs of (22) is, in essence, a Fickian flux of U with the diffusion coefficient dependent on flow variables. In the implied vorticity equation, similar to an eddy viscosity, this term will spawn two type of terms: equivalent Fickian fluxes of the vorticity and baroclinic-like source fluxes that depend on various products of spatial derivatives of A and U. Note that Fickian fluxes always counteract spurious eddies by smearing out point vortices or, in other words, by diluting highly localized regions of elevated vorticity which lead to a wrap-up of the shear layers (cf. [5], chapters 2.6 and 7.2). The role of the "baroclinic" fluxes is unclear a priori. In principle, they can either counteract or act in concert with the spurious source because of the first term on the rhs of (22). The latter seems corroborated by the results of the preceeding section.

4.2. *Modified Schemes*

In the light of the vorticity arguments above, for the schemes that evince spurious eddies, the simplest thing to consider is to accentuate benefits of the Fickian flux and to diminish the magnitude of the eventual "baroclinic" source. Consequently, we selected the FORCE and UHO schemes that originally led to spurious solutions, and repeated the calculations using first order of accuracy to determine right and left states in the WST of the Godunov flux,[10] but retaining higher accuracy in the calculation of the terms E_L and E_R. The results are shown in Fig. 3 and are also compared with the corresponding solutions using third-order of accuracy for the WST. As seen, the modified schemes now provide the same correct solution. It is important to note that the change of accuracy in the WST affects only the spurious vortices, but does not alter the solution in the other flow regions. For example, one can look at the results of the FORCE scheme where in the lower side of the domain the scheme did

[10] Technically, this was achieved by using first-order-accurate interpolation in the WST of the Lax–Friedrichs flux that forms an element of both schemes; cf. sections 2.4 and 2.5.

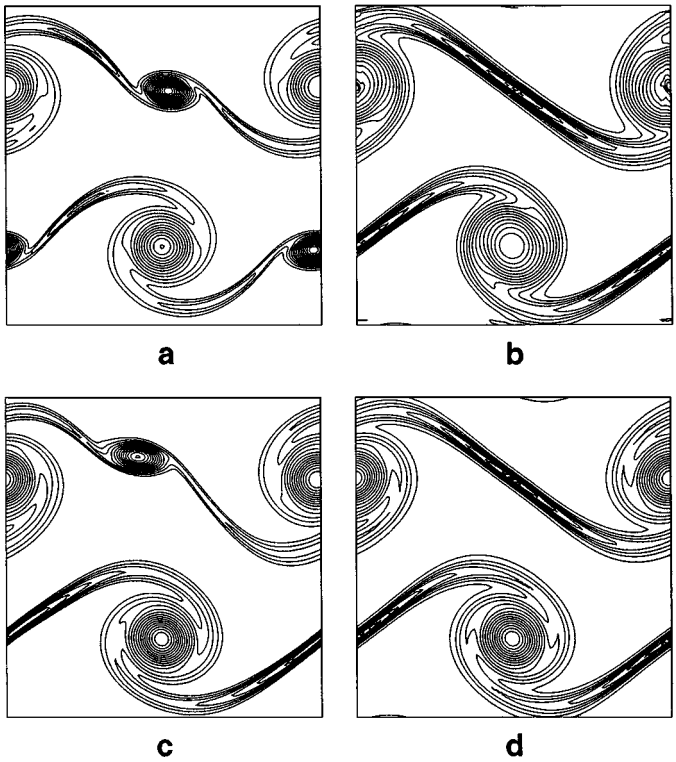

FIG. 3. Correction of the spurious solutions in Godunov-type methods: (a) original UHO-L3 scheme, (b) modified UHO-L3 scheme with first-order-accurate interpolation in the WST, (c) original FORCE-L3 scheme, and (d) modified FORCE-L3 scheme with first-order interpolation in the WST.

not initially result in spurious vortices; after reducing the order of accuracy of the WST, the solution in this flow region remains essentially unchanged. In Table II, we measure the impact of the modifications with the differences (between the original and modified schemes, normalized by the original scheme) of the time-averaged total kinetic energy ($t = 0 \div 1$) and instantaneous total kinetic energy at $t = 1$ (corresponding to Figs. 1–3). For both UHO and FORCE schemes, both measures indicate second-order convergence rate; and for the 256×256 grid, where both the original and modified schemes give the same spurious-eddy-free solution, the results agree closely.

TABLE II

Percentage Difference between the Original and Modified Schemes for the Time-Averaged Total Kinetic Energy ($t = 0 \div 1$) as Well as for the Total Kinetic Energy (Values inside the Brackets) at $t = 1$ (Corresponding to Figs. 1–3)

Grid	UHO	FORCE
64×64	11.08% (18.35%)	4.16% (7.7%)
128×128	4.2% (7.75%)	1.46% (2.89%)
256×256	0.80% (3.20%)	0.34% (0.70%)

TABLE III

RMS Difference between Numerical and Analytic Solution for the Modified and Original, UHO-L3 and FORCE-L3, Schemes for the Problem of an Oscillating Boundary-Layer over a Flat Plate

N_g	Modified FORCE-L3	FORCE-L3	Modified UHO-L3	UHO-L3
32	0.127	$1.70e-3$	$2.57e-2$	$1.55e-4$
64	$3.84e-2$	$1.77e-4$	$1.06e-2$	$1.20e-4$
128	$4.56e-3$	$2.91e-5$	$1.48e-3$	$2.02e-5$
256	$2.91e-4$	$1.33e-5$	$9.75e-4$	$1.16e-5$

Note. N_g denotes number of grid points in the boundary layer.

To assess the effects of the modified WST term on the accuracy of the schemes beyond the vortex-street problem, we have performed two additional, diverse benchmark tests: (a) oscillating boundary layer over a flat plate (alias Stoke's second problem) with known analytic solution [42]; and (b) Burgers' model of turbulence with a random initial velocity profile [43]. For the Stoke's problem, we present in Table III the root-mean-square (rms) error (with respect to the analytic solution of the unit magnitude) for the modified and original UHO-L3 and FORCE-L3 schemes. The errors are clearly smaller for the original schemes, however, for resolutions with 128 points and beyond they are already so small that the differences in the plotted solutions (not shown) are practically indistinguishable. For the Burgers' problem, we measure deviations of various solutions from a high-resolution reference result generated on 20000×16000 points space-time mesh using the FORCE-L3 scheme.[11] In Table IV, we present such deviations for the time-averaged skewness factor using the modified and original FORCE-L3 scheme.[12] In practical terms, both schemes offer similar accuracy.

Although we have demonstrated that the accuracy of interpolation used in the WST of the Godunov flux can affect the production of spurious solutions, it should be borne in mind that the issue of spurious eddies depends on a delicate balance of truncation errors resulting from WST and E_L and E_R components of the Godunov flux. Apparently, this is why RU, LF, and HLLE schemes evince no spurious solutions, even though the WST is defined by the higher-order interpolation. Furthermore, our numerical experiments (not shown) revealed that reducing the accuracy of the WST term in the RU, LF, and HLLE schemes results in overly diffusive solutions for the shear layers. The same effect also follows the use of first-order accurate interpolation in the fluxes E_L and E_R in any of the Godunov-type methods employed in this study.

5. CONCLUDING REMARKS

We have performed a series of numerical experiments using various Godunov-type methods, aiming at the understanding of the numerical mechanisms underlying the formation of spurious vortical structures in underresolved flows. Similar to [2], we have found that

[11] The fidelity of the reference solution was verified by conducting auxiliary reference runs with the RU-L3 and LF-L3 schemes that evince no spurious eddies in the original problem (cf. Table I).

[12] The UHO scheme is unsuitable for this problem because the characteristic-based discretization used for the initial approximation of fluxes has been developed specifically for the advective terms of the Navier–Stokes equations [see (15, 34, 35)].

TABLE IV

Difference between the Numerical and High-Resolution Reference Solution (Obtained on a Space–Time Domain with 20,000 × 16,000 points) for the Time-Averaged Skewness Factor in the Burgers' Problem of Turbulence (Based on a Random Initial Velocity Profile and Periodic Boundary Conditions)

Grid (space × time)	Modified FORCE-L3	FORCE-L3
1000 × 500	28.0%	27.5%
2000 × 1000	7.7%	7.0%
4000 × 2000	0.9%	0.3%
8000 × 4000	0.2%	0.06%

both centered and upwind methods can lead to spurious solutions. Our experiments seem to indicate that the generation of spurious eddies depends solely on the advective scheme. In particular, it depends strongly on how the numerical dissipation is partitioned between different terms of the advective scheme. In the case of Godunov methods, this depends on the detailed form of the Godunov flux.

The truncation error of a discretized vorticity equation is not equivalent, in general, to the vorticity of the truncation error of a similarly discretized momentum equation. A rigorous vorticity analysis of nonlinear approximations such as high-order Godunov-type schemes appears very difficult. We thus have considered an idealized finite-difference scheme and showed how the definition of the advective velocities in the primitive variable formulation of the equations can induce a truncation error vorticity source. Pursuing vorticity arguments for a general Godunov flux, we argued that discretizing the WST in (22) with lower-order interpolation should mitigate erroneous vorticity sources. Numerical experiments corroborated that reducing the order of accuracy in the discretization of WST corrects the numerical solution of those Godunov-type methods which previously led to spurious vortical structures. We hardly claim that the modified fluxes are universally improved versions of the original ones. From the practical viewpoint, however, the effects of extra dissipation arising from the reduced accuracy in the WST appear fairly small, as measured for the discussed vortex-street problem and two unrelated diverse benchmark tests of an oscillating boundary layer over a flat plate and Burgers' turbulence. A better appreciation of the benefits/drawbacks of the nonlinear dissipation of the Godunov-type methods will be acquired by applying the modified and original schemes to a larger number of flow problems of interest to science and engineering.

Although we have succeeded with regaining control over deficient (spurious-eddies-wise) Godunov schemes, by no means do we imply that the problem has been solved to the completion. In particular, the question "why certain schemes evince spurious eddies while others do not" still eludes a scholastic answer. In the class of Godunov schemes, the issue of spurious eddies seems to depend on a delicate ballance of truncation errors resulting from WST and $E_L + E_R$ components of the Godunov flux, and this is the essence of this balance that needs to be understood. The importance of the spurious-eddies issue extends beyond elusive intellectual challenge of the numerical analysis itself. The phenomena of stable and unstable multiple solutions and of spurious steady states, which can occur below and above the linearized stability limit of a numerical method, attract increasing interests in the literature [see (44) and the references therein]. Here, we demonstrated the significance

of the nonlinear dynamical behavior of the numerical scheme used for discretizing the advective term of the Navier–Stokes equations. This is of particular relevance to large-eddy simulation (LES) of turbulent flows, a common tool for research and engineering applications. In LES, spurious solutions arising from the advective term discretization can affect the simulated large-eddy structures and subsequently overwhelm the effects of the small scales accounted for by the subgrid scale model. This should be taken into account in the design of spatio-temporal filters and subgrid scale models.

ACKNOWLEDGMENTS

Stimulating discussions with Joseph Klemp, Len Margolin, and Tito Toro are gratefully acknowledged. Special thanks go to Len Margolin and William Rider for their personal reviews of the manuscript. PKS acknowledges partial support from the U.S. Department of Energy "Climate Change Prediction Program" (CCPP) while conducting this work on the collaborative leave from NCAR (NCAR is sponsored by the National Science Foundation) at the European Centre for Medium Range Weather Forecasts (ECMWF) in Reading UK.

REFERENCES

1. D. L. Brown and M. L. Minion, Performance of under-resolved two-dimensional incompressible flow simulations, *J. Comput. Phys*. **122**, 165 (1995).
2. M. L. Minion and D. L. Brown, Performance of under-resolved two-dimensional incompressible flow simulations II, *J. Comput. Phys.* **138**, 734 (1997).
3. J. B. Bell, P. Colella, and H. M. Glaz, A second-order projection method for the incompressible Navier-Stokes equations, *J. Comput. Phys.* **85**, 257 (1989).
4. A. I. Tolstykh and E. N. Chigirev, On thin shear layers numerical simulation, *J. Comput. Phys.* **166**, 152 (2001).
5. G. K. Batchelor, *An Introduction to Fluid Dynamics* (Cambridge Univ. Press, Cambridge, UK, 1967).
6. D. L. Youngs, Numerical simulations of turbulent mixing by Rayleigh–Taylor instability, *Physica 12D*, **32** (1984).
7. D. Drikakis, Study of bifurcation flow phenomena in incompressible sudden-expansion flows, *Physics of Fluids*, **9**(1), 76 (1997).
8. T. Mullin and K. A. Cliffe, Symmetry-breaking and the onset of time dependence in fluid mechanical systems, in *Nonlinear Phenomena and Chaos*, edited by S. Sarkar (Hilger, Bristol, 1986), pp. 96–112.
9. P. K. Smolarkiewicz and L. G. Margolin, On forward-in-time differencing for fluids: Extension to a curvilinear framework, *Mon. Weather Rev.* **121**, 1847 (1993).
10. P. K. Smolarkiewicz and L. G. Margolin, Variational solver for elliptic problems in atmospheric flows, *Appl. Math. Comp. Sci.* **4**, 527 (1994).
11. P. K. Smolarkiewicz and L. G. Margolin, MPDATA: A finite-difference solver for geophysical flows, *J. Comput. Phys.* **140**, 459 (1988).
12. P. K. Smolarkiewicz and J. A. Pudykiewicz, A class of semi-Lagrangian approximations for fluids, *J. Atmos. Sci.* **49**, 2082 (1992).
13. P. K. Smolarkiewicz and L. G. Margolin, On forward-in-time differencing for fluids: An Eulerian/semi-Lagrangian nonhydrostatic model for stratified flows, *Atmos. Ocean Special* **35**, 127 (1997).
14. D. Drikakis, O. P. Iliev, and D. P. Vassileva, A nonlinear multigrid method for the three-dimensional incompressible Navier-Stokes equations, *J. Comput. Phys.* **146**, 310 (1998).
15. D. Drikakis, Uniformly high-order methods for unsteady incompressible flows, in *Godunov Methods: Theory and Applications*, edited by E. F. Toro (Kluwer Academic, Dordrecht/Norwell, MA, 2001), pp. 263–283.
16. A. J. Chorin, A numerical method for solving incompressible viscous flow problems, *J. Comput. Phys.* **2** 12 (1967).
17. C. L. Merkle and M. Athavale, *Time-accurate unsteady Incompressible Flow Algorithms Based on Artificial Compressibility*, Technical Paper 87-1137 (AIAA Press, Washington, DC, 1987).

18. W. Y. Soh and J. W. Goodrich, Unsteady solution of incompressible Navier–Stokes equations, *J. Comput. Phys.* **79**, 113 (1988).
19. S. E. Rogers and D. Kwak, Upwind differencing scheme for the time accurate incompressible Navier–Stokes equations, *AIAA J.* **28**(2), 253 (1990).
20. S. E. Rogers, D. Kwak and C. Kiris, Steady and unsteady solutions of the incompressible Navier–Stokes equations, *AIAA J.* **29**(4), 603 (1991).
21. C.-W. Shu and S. Osher, Efficient implementation of essentially non-oscillatory shock-capturing schemes, *J. Comput. Phys.* **77**, 439 (1988).
22. J. M. Hyman and M. Shashkov, Adjoint operators for the natural discretizations of the divergence, gradient and curl on logically rectangular grids, *Applied Numer Math.* **25**, 413 (1997).
23. K. W. Morton and P. L. Roe, Vorticity-preserving Lax–Wendroff-type schemes for the system wave equation, *SIAM J. Sci. Stat. Comput*., in press.
24. R. Teman, Navier-Stokes Equations: *Theory and Numerical Analysis* (North-Holland, Amsterdam, 1984).
25. V. V. Rusanov, Calculation of interaction of non-steady shock waves with obstacles, *J. Comput. Math. Phys. USSR* **1**, 267 (1961).
26. E. F. Toro, *Riemann Solvers and Numerical Methods for Fluid Dynamics* (Springer-Verlag, Berlin/New York, 1999).
27. S. F. Davis, Simplified second-order Godunov-type methods, *SIAM J. Sci. Stat. Comput.* **9**, 445 (1988).
28. P. D. Lax, Weak solutions of nonlinear hyperbolic equations and their numerical computation, *Comm. Pure Appl. Math.* **VII**, 159 (1994).
29. B. Einfeldt, On Godunov-type methods for gas dynamics, *SIAM J. Numer. Anal.* **25**(2), 294 (1988).
30. A. Harten, P. D. Lax, and B. van Leer, On upstream differencing and Godunov-type schemes for hyperbolic conservation laws, *SIAM Review* **25**(1), 35 (1983).
31. E. F. Toro, On two Glimm-related schemes for hyperbolic conservation laws, in *Numerical Methods for Wave Propagation*, edited by E. F. Toro and J. F. Clarke (Kluwer Academic, Dordrecht/Norwell, MA, 1998).
32. A. Harten and S. Osher, Uniformly high-order accurate non-oscillatory schemes I, *SIAM J. Numer. Anal.* **24**(2), 279 (1987).
33. A. Harten, B. Engquist, S. Osher, and S.-R. Chakravarthy, Uniformly high-order accurate essentially non-oscillatory schemes, III, *J. Comput. Phys.* **71**, 2 (1987).
34. D. Drikakis, P. A. Govatsos, and D. E. Papantonis, A characteristic-based method for incompressible flows, *Int. J. Num. Meth. Fluids* **19**, 667 (1994).
35. D. Drikakis, A parallel multiblock characteristic-based method for three-dimensional incompressible flows, *Adv. Eng. Software* **26**, 111 (1996).
36. A. Eberle, A. Rizzi, and E. Hirschel, *Numerical Solutions of the Euler Equations for Steady Flow Problems*, Series: Notes on Numerical Fluid Mechanics (Vieweg Weisbaden, 1992), Vol. 34.
37. B. van Leer, Towards the ultimate conservative difference scheme V. Second-order sequel to Godunov's method, *J. Comput. Phys.* **32**, 101 (1979).
38. G. D. van Albada, B. van Leer, and W. W. Roberts, A comparative study of computational methods in cosmic gas dynamics, *Astron. Astrophys.* **108**, 76 (1982).
39. D. Drikakis, L. G. Margolin, and P. K. Smolarkiewicz, On "Spurious" Eddies, in *Proceedings of the ICFD Conference Oxford, UK*, 2001, to appear.
40. R. Kupferman and E. Tadmor, A fast, high-resolution, second-order central scheme for incompressible flows, *Proc. Natl. Acad. Sci. USA* **94**, 4848 (1997).
41. P. L. Roe, Approximate Riemann solvers, parameter vectors, and difference schemes, *J. Comput. Phys.* **43**, 357 (1981).
42. F. M. White, Viscous Fluid Flow (McGraw-Hill, New York, 1974)
43. M. D. Love, Subgrid modelling studies with Burgers' equation, *J. Fluid Mech.* **100**, 87 (1980).
44. H. C. Yee and P. K. Sweby, Dynamical approach study of spurious steady-state numerical solutions for nonlinear differential equations, Part II: Global asymptotic behavior of time discretizations, *Int. J. Comput. Fluid Dyn.* **4**, 219 (1995).